Astron. Astrophys. 246, 231–242 (1991)

ASTRONOMY AND ASTROPHYSICS

# Foreground dust and gas and the extinction curve of the Large Magellanic Cloud

**P. B. W. Schwering * and F. P. Israel**

Sterrewacht Leiden, Postbus 9513, NL-2300 RA Leiden, The Netherlands

Received July 11, accepted December 6, 1990

**Abstract.** We have compared the large-scale distributions of Galactic infrared and H I emission towards the Magellanic Clouds, resulting in estimates of the infrared foreground of the Clouds. For the Galactic gas-to-dust ration by mass we find 420 (+250, −120).

From H I maps, we have also derived maps of the Galactic foreground colour excess towards the Magellanic Clouds on scales of 48 arcmin. Over the LMC surface the foreground reddening is not constant; it ranges from $E(B-V) = 0.07$ to 0.17 mag. For the SMC we find a foreground reddening $E(B-V) = 0.07$ to 0.09 mag. The amplitude of foreground reddening variations is probably much greater on smaller scales. Towards the 30 Doradus region, the mean foreground reddening is quite low. As a result, differences between the 30 Doradus and the average LMC extinction curves are much less than previously suggested.

**Key words:** interstellar medium: gas-to-dust ratio – extinction – Magellanic Clouds: reddening law – foreground reddening – infrared emission: Galactic cirrus

## 1. Introduction

For many applications, especially at optical and ultraviolet wavelengths, knowledge of the amount and distribution of Galactic material in front of the Magellanic Clouds is essential. This distribution is often assumed to be uniform over the face of the Clouds but there is good evidence for considerable variation. For instance, deep visual images of the Clouds by de Vaucouleurs (1955) show a spur-like feature, which has the appearance of a tidal arm coming out of the LMC. It is also clear on IRAS 60/100 μm maps (Israel & Schwering 1986; McGee et al. 1986), but the low radial velocity of its H I counterpart (Cleary et al. 1979; Colomb et al. 1980) betrays its foreground nature. The IRAS maps contain other structures with appearances that suggest a physical relation to the LMC, such as a 'bridge' between the LMC and the Galactic plane, and another thin filament, Yet each of these features has H I velocities attributable to the foreground and they serve to illustrate the complex and non-uniform nature of the Galactic foreground. This complexity is further illustrated by high-contrast prints (Johnson et al. 1982) that show a faint filamentary Hα nebulosity in the Galactic foreground (see also West et al. 1987).

The non-uniform foreground also expresses itself in reddening measurements. Reddening values in specific lines-of-sight found by various authors range from $E(B-V) = 0.04$ to 0.08 mag (LMC) and from 0.01 to 0.07 mag (SMC). Israel & Schwering (1986) used a preliminary version of the IRAS data to estimate a greater range of LMC foreground reddening $E(B-V) = 0$ to 0.15 mag, which must be compared to a *peak* reddening in the LMC itself of $E(B-V) = 0.4$ mag (in 30 Doradus; cf. Isserstedt 1975). Although the Galactic foreground corresponds to a relatively thin veil over the Clouds, its *average* extinction is comparable to the extinction within the Clouds themselves (Koornneef 1984) so that foreground *variations* cannot be neglected when interpreting Cloud observations.

The aim of this paper is twofold. By determining empirical relations between the infrared (warm dust) and H I (gas) foreground emission, the observed H I distribution can be used to separate Galactic infrared emission in front of the Clouds from the infrared emission of the Clouds themselves. Although this result is obtained primarily for use in later papers dealing with the overall infrared properties of the Magellanic Clouds, its implications are briefly discussed.

In the second part of this paper, the same map of Galactic H I emission is converted into a map of the Galactic foreground colour excess distribution on scales of 48 arcmin; the latter is used to reevaluate Magellanic Cloud extinction studies from the literature.

## 2. Data handling and presentation

### 2.1. The infrared data

The foreground features of interest extend over an area about 40° across. In principle, any of three different IRAS products could be used: Spline-I images (van Albada et al. 1985), Skyflux images (IRAS, 1988), and images based on the Zodiacal Observations History File (HOHF; IRAS, 1988). Here, we will use the ZOHF data; the relatively small Skyflux maps are difficult to connect, while Spline I images were made only at 60 and 100 μm.

*Send offprint requests to:* F. P. Israel

* Present adress: Infrared Group, Physics and Acoustics Division, TNO Physics and Electronics Laboratory, P. O. Box 96864, 2509 JG, Den Haag, The Netherlands

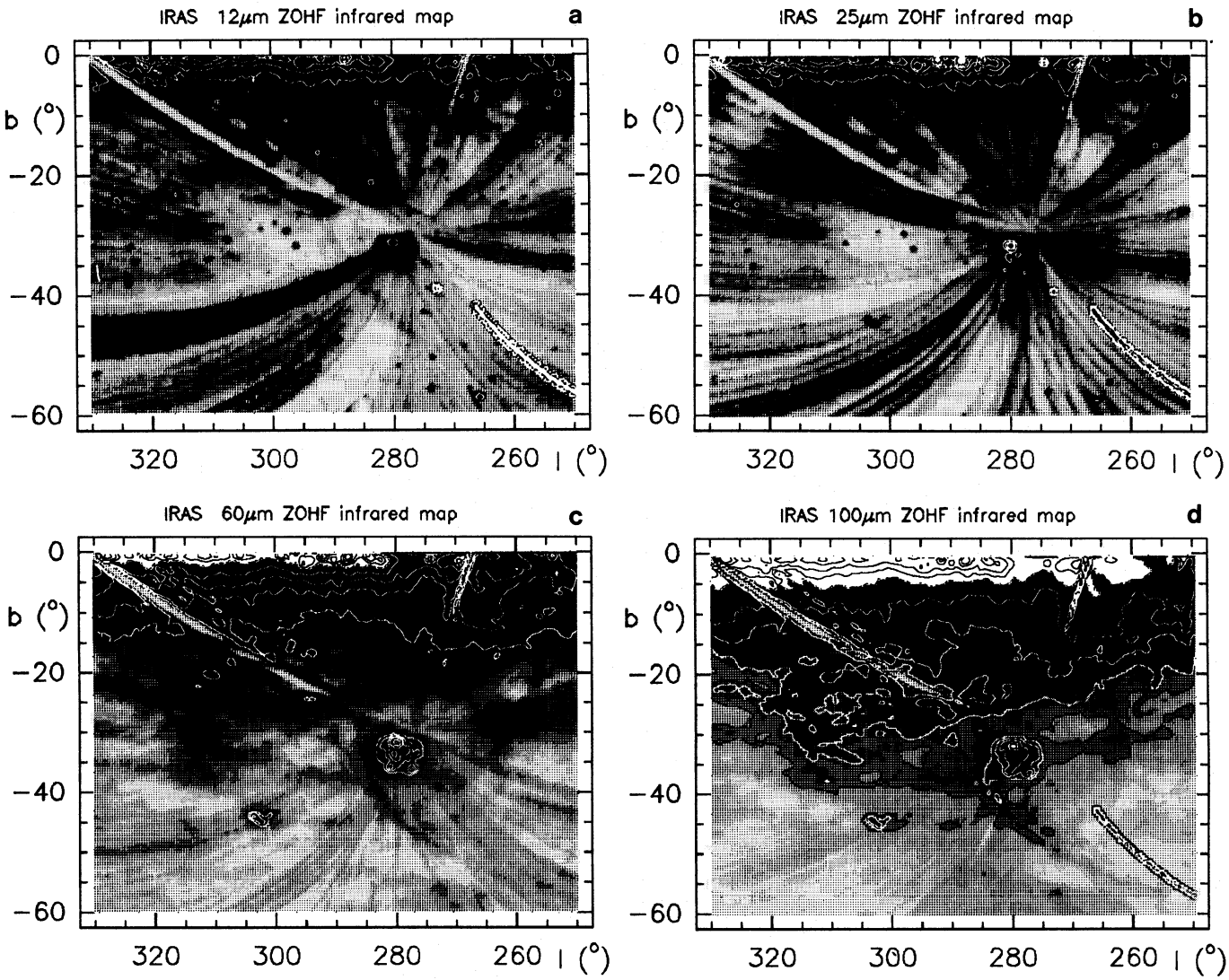


**Fig. 1a–d.** IRAS Zody History File infrared maps at 12, 25, 60 and 100 μm (resolution 48′). The LMC is located at (280°, −33°); the SMC is at (303°, −44°). Grey scales are chosen to emphasize low-level emission. Contours are at 2, 5, 10, 20, 50, 100, 200, 500, 1000 MJy sr$^{-1}$ in all four bands

In his study of Galactic infrared emission, Deul (1988) combined the ZOHF scan-data into intensity maps in Galactic coordinates and subtracted a model of the Zodiacal Light (Deul & Wolstencroft 1988). At the South Ecliptic Pole, close to the Magellanic Clouds, subtraction residuals are negligible compared to residual instrumental stripes (typically 0.5, 0.5, 0.2 and 0.1 MJy sr$^{-1}$ at 12, 25, 60 and 100 μm respectively). These maps, and all other infrared maps in this paper, assume an intrinsic source spectrum $f_\nu \propto \nu^{-1}$. Figure 1 shows these maps convolved to the H I map resolution of 48 arcmin with a pixel size of 15 arcmin. The corresponding linear resolutions are $<1.4$ pc at local distances $<100$ pc, and 770 pc at 55 kpc (the distance of the Clouds). Note the radial instrumental striping pattern centered on the South Ecliptic Pole, and the strong Galactic plane emission located at the top. The features mentioned in the introduction can be recognized in the 60 and 100 μm maps. The two filaments extend from the lower left corner of the LMC at (285°, −35°), and the 'bridge' is seen at (270°, −30°); they are near or below the striping level in the 12 and 25 μm maps.

### 2.2. *The* H I *data*

We have used the large-scale H I survey (Cleary et al. 1979) made with the 18 m Parkes radiotelescope. The survey covers the Southern Hemisphere at $\delta < -30°$, and $b > |10°|$, with a HPBW of 48 arcmin and velocity sampling of 7 km s$^{-1}$. It consists of drift scans at constant declination and is spatially undersampled. The velocity range includes that of the Magellanic Clouds. In order to obtain maps with a 15 arcmin pixel size we have subjected the original data to a $4\times4$ Lagrangian interpolation. We then integrated the profiles over the velocity range $-38 < V_{LSR} < +38$ km s$^{-1}$, including essentially all Galactic foreground H I (Colomb et al. 1980), but excluding H I emission from the Magellanic Clouds (McGee & Newton 1981; Rohlfs et al. 1984). We did not use a larger range in order to avoid inclusion of uncorrelated signals, which would result in a higher noise level. Integrated H I column densities (Fig. 2a) follow from $N$(H I) ($10^{20}$ H-atoms cm$^{-2}$) $= 0.018\,\eta_{mb}\,(\Delta v/\mathrm{km\,s^{-1}})\,\sum(T_A/K)$ and the Parkes 18 m telescope main beam efficiency $\eta_{mb} = 0.85$. We assume implicitly

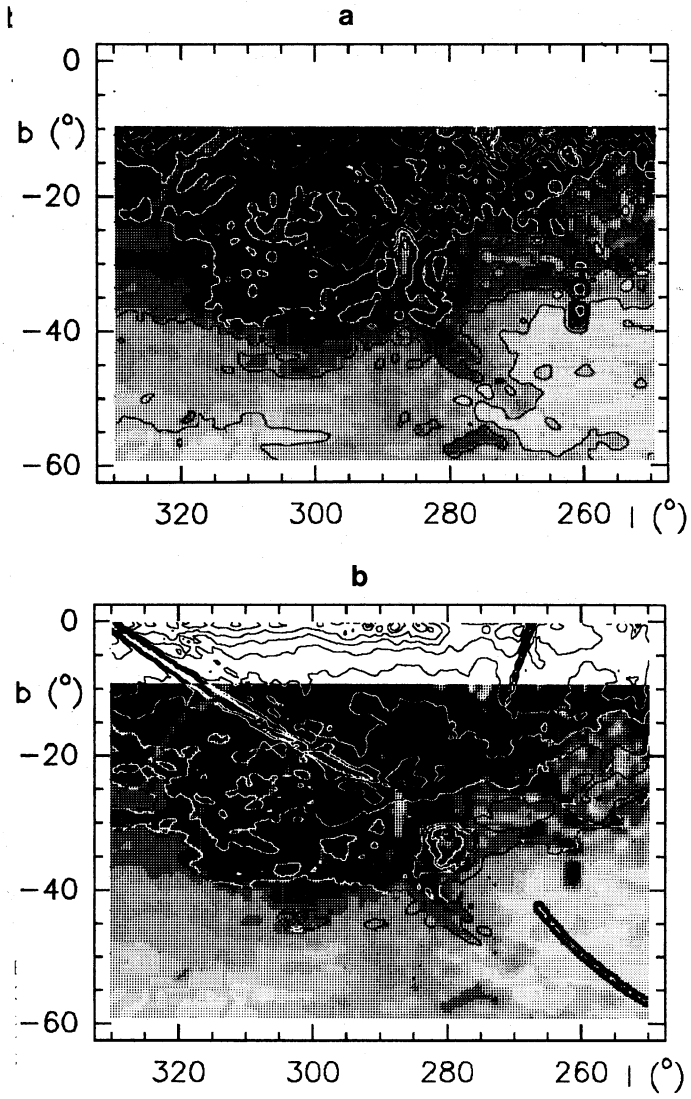


**Fig. 2.** **a** H I column density map; low-level intensities are emphasized in the half-tone representation. Contours are at 2, 4, 8, 12, 16, $10 \times 10^{20}$ H-atoms $cm^{-2}$. **b** Overlay of infrared 100 μm contours on H I column density halftone map. Infrared contours and H I grey scales are identical to those in Figs. 1d and 2a

that the H I emission is optically thin, which is probably correct at these Galactic latitutes (cf. Strong et al. 1982; McGee et al. 1986). Comparison of our map to one integrated over the full velocity range (Deul 1988) shows that our velocity interval indeed contains 85–90% of the total velocity-summed H I emission. Since the latter may contain uncorrelated signals, we conclude that our map is accurate to within about 10%.

A potential problem is contamination of the H I signal by stray radiation entering through antenna sidelobes and the spillover lobe of the 18 m telescope. Heiles & Cleary (1979) estimate sidelobe contamination to be negligible. We have used maps of the large-scale Galactic H I distribution and the properties of the 18 m telescope to estimate that spillover contamination at the location of the Magellanic Clouds (and indeed over most of the field) is unlikely to correspond to an equivalent hydrogen column density of more than $10^{19}$ H $cm^{-2}$. For comparison, this corresponds to the lower stray radiation levels measured by Lockman et al. (1986) with the NRAO 43 m telescope. As the H I column densities found above are typically of order $10^{20}-10^{21}$ H $cm^{-2}$, we conclude that, at the Galactic longitude and latitude of the Magellanic Clouds, spillover contamination is not a major contributor to the observed signal.

Figure 2b shows 100 μm infrared contours superposed on the H I column density distribution represented by grey scales. There is a good overall correlation of the two distributions; note that the Magellanic Clouds are located on IR and H I gradients. The Bar and the 30 Doradus region in the LMC are seen through a 30 per cent "hole" in the foreground H I. The H I feature just below the SMC results from H I structure in the scan direction at velocities where individual H I scans show only noise. As the feature does not appear on the original maps of Cleary et al. (1979), it is an artifact probably due to noise blow-up in the map processing.

## 3. The cirrus infrared foreground at 60 and 100 μm

The stellar infrared foreground of the Magellanic Clouds is significant only at 12 μm, contributing 3 per cent (LMC) and 10 per cent (SMC) to the total integrated flux density respectively. Data on the stellar foreground of the Magellanic Clouds are summarized in Table 1.

The more important Galactic cirrus infrared foreground of the Clouds is determined by extrapolation from the observed H I

**Table 1.** Parameters of stellar infrared foreground emission

| IRAS IR band | LMC | | | | | SMC | | | | |
|---|---|---|---|---|---|---|---|---|---|---|
| | $N_*$ | $F_\nu$ (Jy) | $f_\nu^{max}$ (Jy) | $f_\nu^b$ (Jy) | $f_\nu^t$ (Jy) | $N_*$ | $F_\nu$ (Jy) | $f_\nu^{max}$ (Jy) | $f_\nu^b$ (Jy) | $f_\nu^t$ (Jy) |
| 12 | 253 | 130 | 8.2 | 0.51 | 0.51 | 43 | 17 | 2.6 | 0.40 | 0.40 |
| 25 | 154 | 51 | 4.6 | 0.33 | 0.20 | 12 | 3.5 | 0.8 | 0.29 | 0.08 |
| 60 | 4 | 3.2 | 1.2: | 0.80: | 0.01 | 1 | 0.4 | 0.4 | 0.40 | 0.01 |
| 100 | 0 | – | – | – | – | 0 | – | – | – | – |

*Notes to Table 1:* Columns 2 and 7 give the total number $N_*$ of stellar foreground objects detected. Flux densities are given in columns 3–6 and 8–11: $F_\nu$ is the total flux density of all stars; $f_\nu^{max}$ is flux density of the brightest star in the sample; $f_\nu^b$ is the average flux density per star per band; $f_\nu^t$ is the average flux density normalized to the total number of stars detected in the 12 μm band. All flux densities assume an intrinsic spectrum $f_\nu \propto \nu^{-1}$.

foreground. We assume a constant gas-to-dust ratio and the absence of foreground $H_2$. The survey by Dame and Thaddeus (1987) shows very little CO detected at high Galactic latitudes: $I_{CO} < 5\,K\,km\,s^{-1}$ at $b > |5°|$, while in the Galactic plane $I_{CO} > 50\,K\,km\,s^{-1}$. The same result was obtained by May et al. (1990) for high latitudes in the third Galactic quadrant. No local high latitude molecular clouds are known in this part of the sky. Thus, there is probably also very little $H_2$ in this region.

### 3.1. *Relation of infrared to* H I *emission*

It has been suggested that the Galactic diffuse 12 and 25 μm emission at Magellanic Cloud latitudes is caused by very small grains (radius 3–10 Å) heated to high non-equilibrium temperatures ($T(12/25\,\mu m) = 300–1500\,K$) by absorption of single high-energy UV photons (cf. Puget et al. 1985; Draine & Anderson 1985; Cox et al. 1986). The similarity of the Galactic 12 and 100 μm emission maps suggests that these small grains are well-mixed with the larger grains, and thus with H I. However, at least on scales of 1°, we could not find the expected good relation between $I(12\,\mu m)$ and $N(H\,I)$, possibly because of the disturbing effect of instrumental striping and perhaps residual Zodiacal Light. Infrared emission corrected for temperature dependent emissivity only yields a marginally better result. Thus, we have found no evidence that the distributions of hot, small grains and H I in the Galactic foreground are similar.

The distribution of the cooler dust grains responsible for the 60/100 μm emission should be very similar to that of H I (Cox et al 1986). Thus, 60/100 μm, emission should be well-correlated with H I emission, especially since Galactic far-infrared and H I emission have approximately equal scale heights (Burton & Deul 1987). Figure 3 indeed indicates a reasonably good correlation on scales of 1°. The relation found here between H I and IR emission is, however, not linear. Power-law fits of the form $I_\nu(Gal) = \alpha_\nu N_{H\,I}^{\beta_\nu}(Gal)$ yield $\alpha_{100} = 0.08 \pm 0.05$, $\beta_{100} = 1.8 \pm 0.4$ ($N(H\,I) = 0.3–2.0\ 10^{21}\,H\,cm^{-2}$) and $\alpha_{60} = 0.0007$ $(+0.0007, -0.0004)$, $\beta_{60} = 3 \pm 1$ ($N(H\,I) = 1–2\ 10^{21}\,H\,cm^{-2}$). We note that the formal errors in $\beta_\nu$ are much smaller, but that possible systematic errors raise them to the values quoted. These nonlinearities cannot be explained by H I zerolevel uncertainties or stray radiation contamination (cf. Sect. 2.2; Heiles & Cleary 1979). By plotting linear values instead of the logarithmic values shown, we verified that the nonlinearity is not caused by a constant base-offset in the infrared data (which might be of order 0.1–0.2 $MJy\,sr^{-1}$). We note that nonlinear ('curved') relationships between far-infrared and H I emission can also be recognized in other studies. For instance, a clear non-linearity is obvious from the studies of cool gas and dust in the Galaxy by Burton and Deul (1987, Fig. 9; see also Deul & Burton 1990) and in Ophiuchus by de Geus (1988, p. 77/78). The precise relationship appears to depend both on the Galactic region studied and on the range of infrared/H I intensities considered. Moreover, Bloemen et al. (1990) find that the infrared emissivity per H atom increases significantly with decreasing Galactic radius. Finally, we note that Figs. 4 and 5 by Boulanger & Perault (1988), covering a similar range of H I and infrared intensities, likewise suggest a mild nonlinearity. However, our conclusion differs from

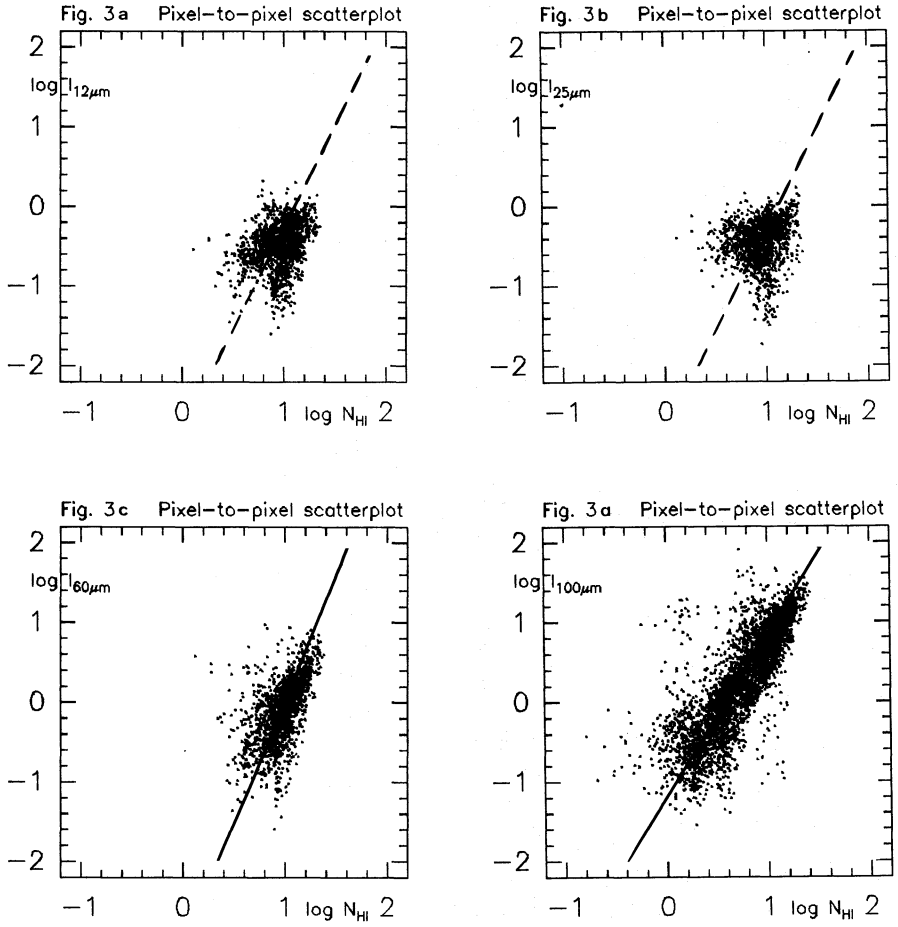


**Fig. 3a–d.** Scatter diagrams of infrared emission ($MJy\,sr^{-1}$) versus H I column density ($10^{20}\,H\,cm^{-2}$). *Solid* and *dashed lines* show least squares fits (see text). Pixels have been averaged over $1° \times 1°$ areas; only in Fig. 3d all available pixels were used

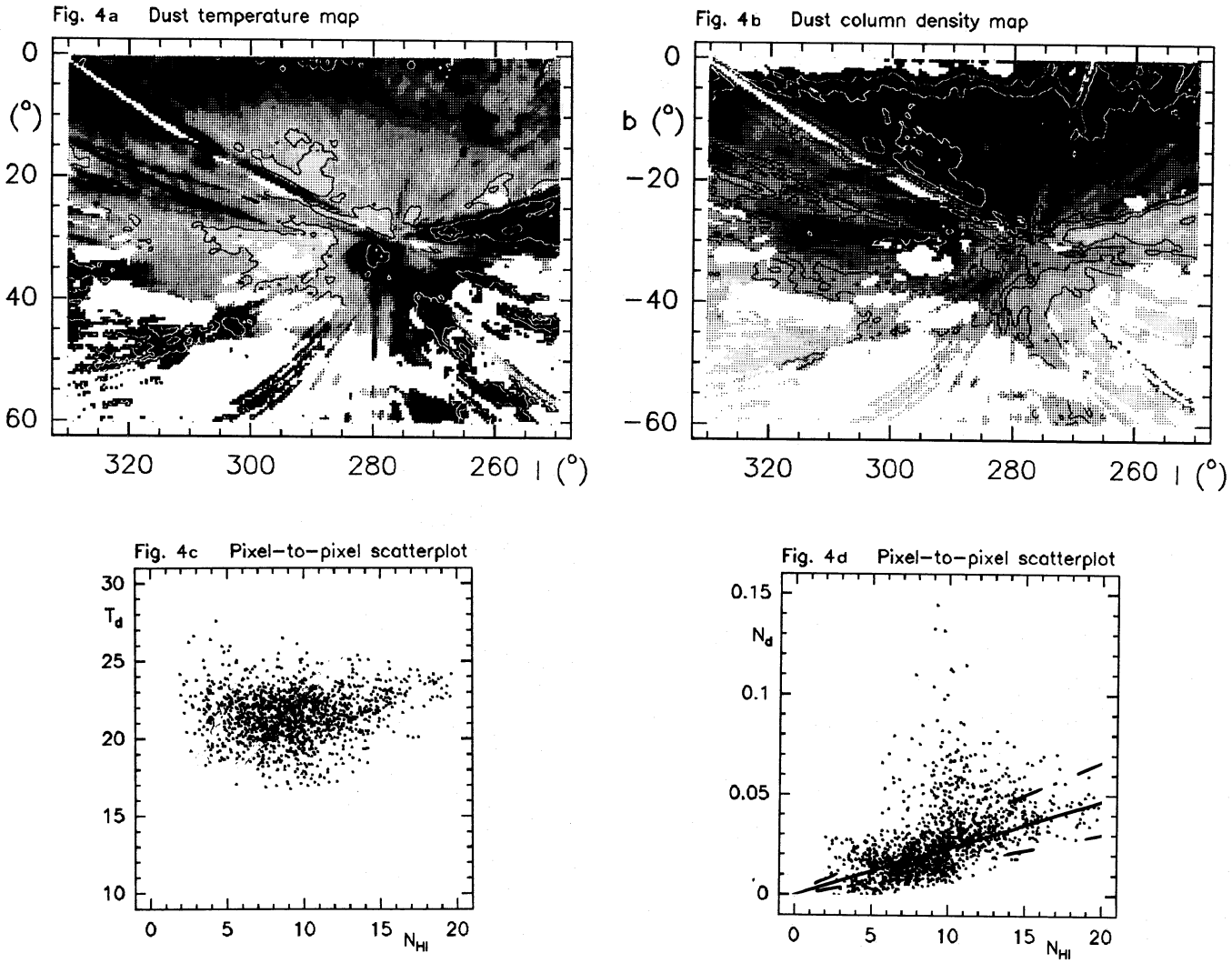


**. 4.** **a** 60/100 μm dust temperature map assuming an emissivity with $n = \lambda^{-1.5}$ wavelength dependence. An intensity cut-off has been applied at 0.2 MJy sr$^{-1}$. ey scales emphasize low temperature regions. Contours are at 20, 30, 40, 50, 60, 70 K. **b** Dust column density map derived from the 100 μm intensity and dust iperature maps. Grey scales emphasize low dust column densities. Contours are at 0.1, 0.5, 1, 5, 10 $10^{18}$ H cm$^{-2}$. **c** Scatter diagram of $T_d$ (K) versus $N$(H I) $^{20}$ H cm$^{-2}$); pixels were averaged over 1° × 1° areas. **d** Pixel-to-pixel scatter diagram of $N_d$ versus $N$(H I) in units of $10^{20}$ H cm$^{-2}$, averaged over 1° × 1° areas. *Solid* corresponds to relation given in text. *Dashed lines* indicate the range of error

it reached by Boulanger & Perault (1988) on the basis of igitude averaged latitude profiles (cf. their Fig. 1). We note that least some variation in the $I_{100}/N$(H I) ratio is to be expected ause of dust temperature variations, which are less apparent in dies dealing with emission averaged over large areas.

### . *Dust grain temperatures and column densities*

om the 60/100 μm map we have derived mean line-of-sight dust iperatures $T_d$, assuming emissivities proportional to $\lambda^n$, with = −1.5 and applying a brightness cutoff at 0.2 MJr sr$^{-1}$ in order avoid noise blow-up. The intensity of the far infrared emission m dust is strongly dependent on the temperature of the larger ins ($I_\nu \propto T_d^{5.5}$): a 15% temperature increase from 20 to 23 K ubles the observed intensity. A map of the dust temperature tribution is shown in Fig. 4a. The LMC, the SMC and the lactic plane have higher temperatures than the general Galactic eground. The relation between $T_d$ and $N$(H I) is shown in Fig. 4b. In this Figure we have eliminated points corresponding to obvious stripe-regions (all points with $b < -40°$ and points in the region $250° < l < 280°$, $-30° < b < -25°$) which yield unrealistically high temperatures $T_d > 30$ K. The mean foreground temperature near the LMC is fairly constant at $T_d = 21 \pm 2$ K, which is very close to the temperatures found for thin, high-latitude clouds by de Vries (1986) in a more elaborate analysis. A further analysis shows that averaged over longitude (after deletion of instrumentally affected areas) slowly $T_d$ decreases away from the Galactic plane (Table 2). At latitudes below $b = -35°$, $T_d$ increases again but this result is less reliable because the relative weakness of $I_{60}$ introduces a large error in $T_d$. The behaviour of $T_d$ for $-10^0 < b < -35°$ is consistent with an increase in the Galactic radiation field strength both towards the Galactic plane (cf. Bloemen et al. 1990) and towards the Galactic centre. If the increase in $T_d$ at $b < -35°$ is not an artifact caused by an offset in $I_{60}$, it could be related to the presence of the presumably local H I cloud complex between $l = 280°$ and $l = 315°$ that extends down to

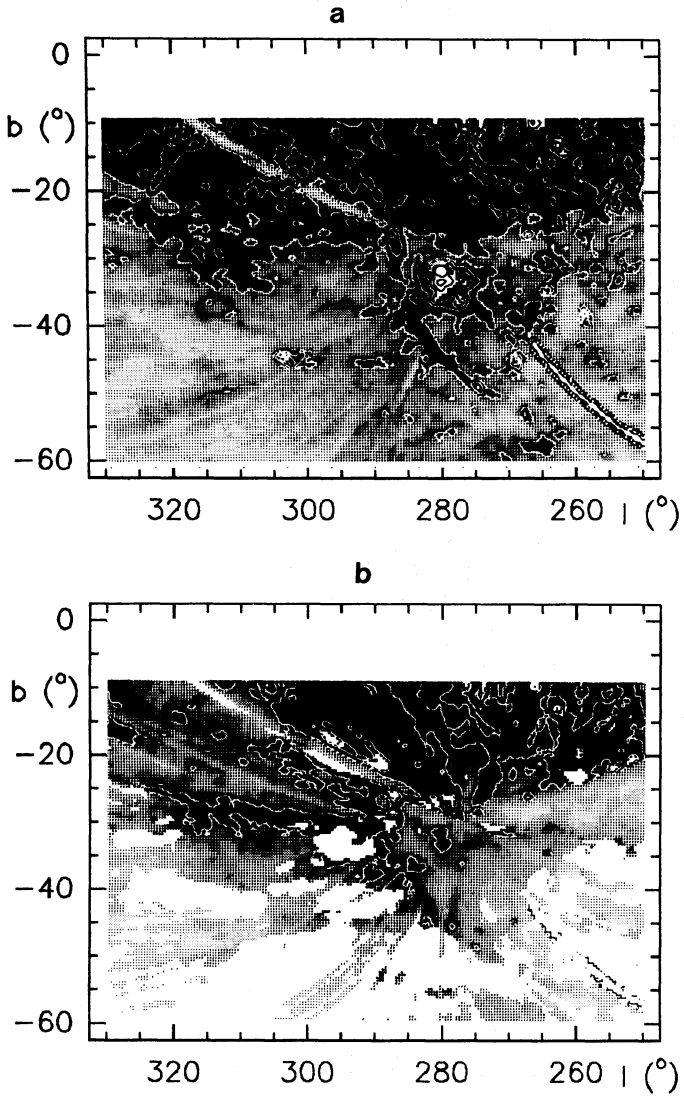


**Fig. 5** **a** Ratio of 100 μm emission to H I column density with contours at 0.5, 1, 2, 5, 10 MJy sr$^{-1}$)/($10^{20}$ H cm$^{-2}$). **b** Ratio of dust to H I column density $N_d/N$(H I) with contours at 0.0025, 0.0075 and 0.02

**Table 2.** Longitude-averaged H I column densities and dust temperatures

| Latitude (°) | $N$(H I)[a] ($10^{20}$ H cm$^{-2}$) | $T_d$ ($n=1.5$) (K) |
|---|---|---|
| −10 | 13.2±4.8 | 23.5±0.7 |
| −10–15 | 11.8±3.3 | 22.4±0.9 |
| −15–20 | 9.1±2.5 | 21.6±0.9 |
| −20–25 | 9.1±2.8 | 21.3±1.0 |
| −25–30 | 8.6±2.7 | 20.7±1.1 |
| −30–35 | 8.3±1.7 | 20.5±1.1 |
| −35–40 | 7.4±1.4 | 20.7±1.2[b] |
| −40–45 | 4.7±1.1 | 22.0±1.5[b] |
| −45–50 | 3.5±1.1 | 22.8±2.7[b] |

[a] Errors given represent spread of $N$(H I) and $T_d$ values present in this latitude range.
[b] Values may suffer from significant systematic error due to possible $I_{60}$ offset.

$b=-35°$, just the latitude of minimum temperature. Alternatively, an increasing presence of small grains contributing to the emission at 60 μm beyond $b=-35°$ (see below) would lead to increasing overestimates of $T_d$, likewise explaining the nominally observed behaviour. The present data do not allow us to discriminate between these possibilities.

The use of emissivity-corrected (temperature corrected) 60 and 100 μm intensities as a measure of dust column densities is justified only if the temperature is constant throughout the line-of-sight, and if grain properties do not vary over the field or in the line-of-sight. We assume the first to the case, because the temperature distribution across the sky shows relatively little variation. Also, from the decomposition method described by Schwering (1988) we may estimate that line-of-sight variations in $T_d$ might increase $N_d/N$(H I) by at most about 30 per cent. For the moment we will assume variation in (small) grain properties to be negligible, at least for $b>-35°$ (but see below).

We have calculated dust mass column densities $M_d$ from temperature-corrected 100 μm intensities and an assumed mass absorption coefficient $\kappa_{100}=40$ cm$^2$ g$^{-1}$ (cf. Hildebrand 1983, for $n=1.5$). The resulting mass column density map is shown in Fig. 4b. In which column densities are expressed as the number of H atoms that correspond in mass with the calculated dust column (i.e. $N_d=M_d/m$(H I)). Column densities are high in the Galactic plane and decrease towards more negative latitudes. The LMC and SMC do not stand out, as they have a $T_d$ considerably higher than the foreground, and apparently much lower $N_d$. On scales of a degree, the H I distribution correlates fairly well with the dust column density distribution as shown in Fig. 4d. In that Figure, the points with $N_d>0.04$ between at $N$(H I) = (0.5 − 1.1) $10^{21}$ H cm$^{-2}$ correspond to a noisy low-temperature region at the upper left of the LMC; they have a relatively large error.

### 3.3. *The foreground gas-to-dust ratio*

We have used the area free from Magellanic Cloud infrared emission to obtain an estimate for the mean Galactic foreground gas-to-dust ratio by mass, $\langle N(\text{H I})/N_d\rangle$, under the assumption that dust and gas are well mixed. From Fig. 4d we find $\langle N(\text{H I})/N_d\rangle = 420$ (+250, −120), for the range $N$(H I) = 0.3–2.0 $10^{21}$ H cm$^{-2}$. Using the same method, F. van Roermund (priv. comm.) found a similar value of 350 ± 50 for the Scorpius region close to the Galactic plane. The formal error reflects the scatter in Fig. 4d, which is mainly determined by bad points and artifacts in the infrared and H I data (Sect. 2). It does not take into account systematic effects introduced by uncertainties in dust particle properties (see Draine & Anderson 1985; Hildebrand 1983). Although these are hard to quantify, we note that especially the value of the mass absorption coefficient $\kappa_{100}$ is uncertain by a factor of two (Hildebrand 1983). We note that our value for the Galactic gas-to-dust ratio is three times higher than classical values (150 ± 50, cf. Osterbrock 1973; Hildebrand 1983; Savage & Mathis 1979), but in view of the uncertainties the significance of this result is not clear.

In Fig. 5b we show a map of the (gas-to-dust ratio)$^{-1}$ (corresponding to Fig. 4d). Figure 5a (corresponding to Fig. 3d) shows the relation between $N$(H I) and $I_{100}$. In particular the aforementioned H I feature between $l=280°$ and $l=315°$ has relatively little dust, which also must be relatively cold. This is in contrast to the Galactic H I filaments mimicking LMC tidal arms that are not very warm, but nevertheless are easily identified in Figs. 5a and 5b. The lowest gas-to-dust ratios appear near the Galactic plane. Gas-to-dust ratios appear to be relatively high a

$b < -30°$, but this is at least partly due to the uncertain, relatively high derived dust temperatures.

Actual gas-to-dust ratios could be lower if there is an additional presence of cold dust ($T_d = 15$ K, cf. Cox et al. 1986). We would need almost three times the amount of observed warm dust in order to obtain $\langle N(\mathrm{H\,I})/N_d \rangle = 150$, which could indeed just have escaped detection. In that case, however, this rather cold dust should exist primarily at the southernmost latitudes, where the nominally observed dust temperatures are increasing.

Note that small grains may contribute significantly to the observed 60 μm emission but not to the 100 μm emission, so that actual dust temperatures will then be lower than derived here. As a consequence, gas-to-dust ratios would also be lower. In order to find $\langle N(\mathrm{H\,I})/N_d \rangle = 150$, the observed 60 and 100 μm intensities require an average large-grain temperature $T_d = 18$ K rather than 21 K, and thus a contribution to the total 60 μm emission by small grains of as much as 45%. Again, Fig. 5b would indicate a small grain contribution smallest near the Galactic plane and largest at the lower latitudes. This is perhaps not unlikely: it would imply that the Solar Neighbourhood dust is mostly of a cirrus nature, rich in small grains, whereas dust at smaller Galactic radii contains a larger 'H II region' dust component.

Finally, it is important to note that the *absolute* value of the gas-to-dust ratio has no influence on the extrapolation of the Galactic foreground over the Clouds. Nor is this the case for other applications such as comparison with gas-to-dust ratios in other galaxies determined in the same way, as long as the overall properties of dust grains are similar.

### 3.4. *The infrared foreground of the clouds*

The variation in dust temperature of the Galactic foreground is small, but just large enough to cause variations of about a factor of two in the ratio $I_{100}/N(\mathrm{H\,I})$. Thus, an extrapolation of the Galactic foreground over the Magellanic Clouds based on $\langle N_d/N(\mathrm{H\,I}) \rangle$ is to be preferred over one based on $\langle I_{100}/N(\mathrm{H\,I}) \rangle$.

We have constructed a map of the Galactic foreground infrared emission at 60 and 100 μm by scaling the $N(\mathrm{H\,I})$ map with $\langle N_d/N(\mathrm{H\,I}) \rangle = 1/420$ and convolving this with the Planck function $B_\nu$ at the derived line-of-sight dust temperatures $T_d$ ($I_\nu^{\mathrm{for}} = (N(\mathrm{H\,I})/\langle N(\mathrm{H\,I})/N_d \rangle)\, m(\mathrm{H\,I})\, \kappa_\nu B_\nu(T_d)$). The smoothest transition to the surrounding foreground with directly determined $T_d$ is obtained for $T_d = 21.5$ K. For the assumed value of $\langle N_d/N(\mathrm{H\,I}) \rangle$ this corresponds to approximately $I_{100}/N(\mathrm{H\,I}) = 0.9$ MJy sr$^{-1}$/($10^{20}$ H atoms cm$^{-2}$). The H I-predicted foreground infrared maps are shown in Figs. 6a and 6d, which contain structure down to the resolution limit of 48 arcmin. We have subtracted these maps from the observed maps (Figs. 6b and 6e); Figures 6c and 6f show the ratio of predicted to observed infrared foreground emission at 60 and 100 μm. Figures 6b and 6e show that the results are quite satisfactory, with small residuals of about 0.1 MJy/sr near the LMC (positive at 60 μm, negative at 100 μm). These values are smaller than the estimated error in the baselevel of the full-resolution AO maps presented by Schwering (1988). Comparison of this foreground determination with a planar fit shows some differences. The simple planar fit underestimates the 60 μm foreground over the South of the LMC (30 Dor and Bar), and overestimates the foreground over the North. On average the 60 μm planar fit is quite good and yields the same foreground as the H I method. At 100 μm the planar foreground of the whole LMC is too low, except towards the Bar and 30 Dor; the planar foreground is now on average 20% lower than that derived from the H I.

**Table 3.** Average foreground towards the Magellanic Clouds

| Quantity (unit) | LMC foreground | SMC foreground |
|---|---|---|
| *Extinction*[a]: | | |
| $E(B-V)$ mag | $0.07-0.17$ | $0.07-0.09$ |
| $E(B-V)/I_{60}$ | $0.20\pm0.08$ | $0.27\pm0.09$ |
| $E(B-V)/I_{100}$ | $0.04\pm0.02$ | $0.07\pm0.03$ |
| *Atomic hydrogen*[b]: | | |
| $N(\mathrm{H\,I})$ $10^{20}$ H cm$^{-2}$ | $5.6\ \pm2.0$ | $4.3\ \pm1.3$ |
| $\langle N(\mathrm{H\,I})/N_d \rangle$ (mass) | $420+250,\ -120$ | |
| *Infrared emission*[b,c]: | | |
| $f_{60}$ Jy | $10000\pm2000$ | $1400\pm400$ |
| $f_{100}$ Jy | $68000\pm12000$ | $5800\pm1500$ |
| $I_{60}$ MJy sr$^{-1}$ | $0.5\ \pm0.1$ | $0.3\ \pm0.1$ |
| $I_{100}$ MJy sr$^{-1}$ | $3.5\ \pm0.6$ | $1.2\ \pm0.3$ |

[a] The average *internal* colour excess is $E(B-V) = 0.07\pm0.04$ mag (LMC) and $0.03\pm0.03$ mag (SMC) (Koornneef 1984).
[b] The errors indicate the range of variation in the parameters listed. Infrared foreground intensities are corrected for Zodiacal Light contribution.
[c] The average infrared foreground flux density was found by summing pixels, by fitting the foreground and by using the predicted foreground. The ratio $I_{60}/I_{100} = 0.18-0.19$ suggests that these are a good values.

Table 3 summarizes the Galactic foreground data. The 60 μm foreground flux density is 10–20% of the integrated Clouds flux density; at 100 μm it is 30–40%. The higher percentages are for the SMC, which is fourteen times weaker at 60 and 100 μm than the LMC. SMC foreground intensities are 0.3–0.6 times those of the LMC. As mentioned in the introduction, the infrared foreground determined here will be used in later papers dealing with the Magellanic Clouds exclusively.

## 4. The Galactic foreground extinction of LMC and SMC

Using the H I maps from Sect. 2, and assuming no $H_2$ to be present, we have calculated the colour excess in the Galactic foreground of the Magellanic Clouds from $E(B-V)$ (mag) $= 0.17\ 10^{-21} N(\mathrm{H\,I})$ H cm$^{-2}$ as derived for the Solar Neighbourhood (Bohlin et al. 1978; Savage & Mathis 1979). Note that this is independent of the results obtained in the previous sections. The resulting $E(B-V)$ maps are shown in Fig. 7, while Fig. 8 shows overlays of LMC and SMC 100 μm emission contours onto $E(B-V)$ grey scales in Galactic coordinates. Ignoring the spurious feature discussed in Sect. 2.2, we find a relatively smooth SMC foreground: although the field is characterized by a gradient from $E(B-V) = 0.06$ to 0.10 mag, the mean foreground towards the SMC itself is $E(B-V) = 0.06$ mag for the southwest Bar, and about 0.07 mag for the remainder. Only in the extreme south and east do we find $E(B-V) = 0.08$ mag. The LMC foreground (mean $E(B-V) = 0.10$ mag) shows significant variations down to the resolution limit of 48 arcmin. The North has $E(B-V) = 0.09-0.11$, while Doradus and most of the Bar have $E(B-V) = 0.06-0.08$. The South has the highest $E(B-V) = 0.13-0.17$ mag. Possible systematic errors in $N(\mathrm{H\,I})$

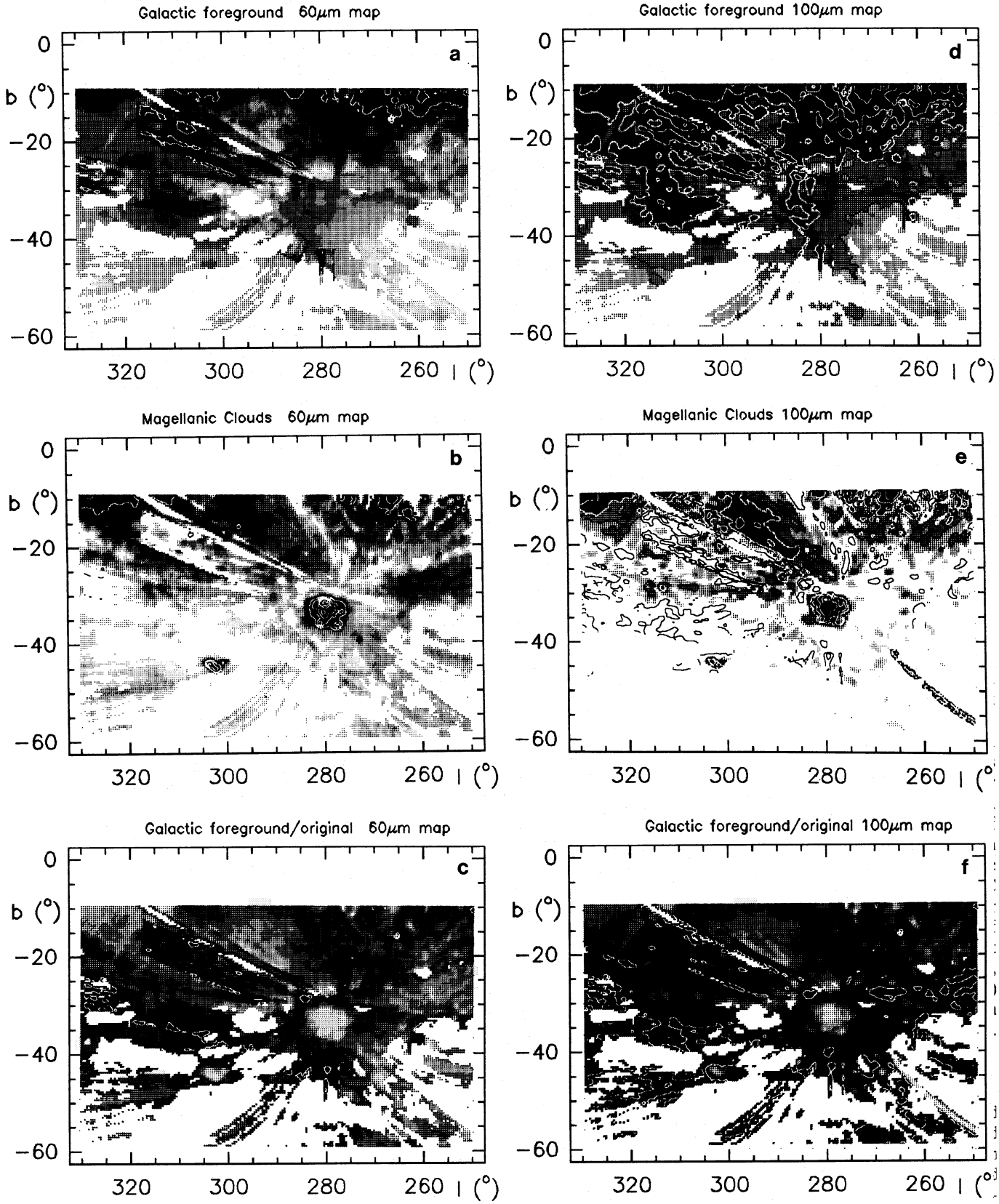


**Fig. 6.** **a** Map of Galactic foreground emission at 60 μm. Contours and grey scales as in Fig. 1c. **b** Magellanic Cloud infrared emission and residuals of Galacti foreground at 60 μm. Contours and grey scales as in Fig. 1c; additional contours at −5, −2 MJy sr$^{-1}$. **c** Map of relative Galactic foreground emission at 60 μm; gre scales as in Fig. 1c; additional contours at 2, 5, 10. **d** As Fig. 6a, for 100 μm emission. Contours and grey scales as in Fig. 1d. **e** As Fig. 6b, for 100 μm emissio Contours and grey scales as in Fig. 1d; additional contours at −5, −2 MJy sr$^{-1}$. **f** As Fig. 6c, for 100 μm emission

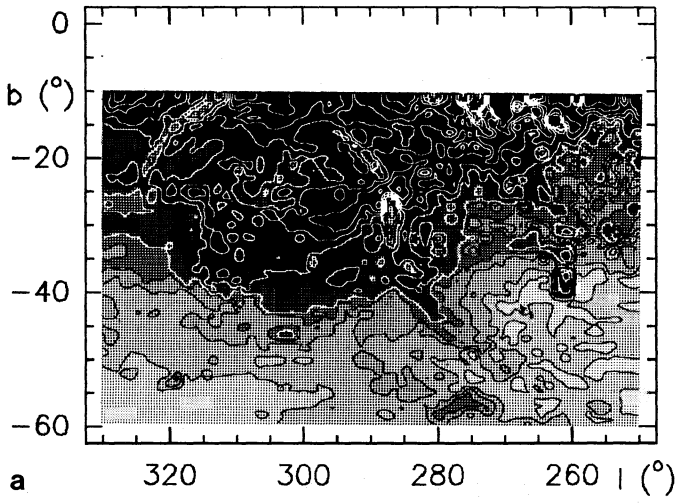


**Fig. 7. a** Map of Galactic foreground colour excess $E(B-V)$. Grey scales emphasize low values of $E(B-V)$. Contours are at 0.02, 0.04, 0.06, 0.08, 0.10, 0.14, 0.18, 0.22, 0.26, 0.30 mag

(Sect. 2.2) correspond to an uncertainty of at most 0.01 mag in $E(B-V)$. The above variation in foreground extinction is only a lower limit: with our crude resolution of 48 arcmin, we have smoothed actual small-scale variations, and reduced their amplitude to a potentially great degree.

The average foreground $E(B-V)$ approaches the higher values published previously (SMC: $0.04 \pm 0.03$, Azzopardi & Vigneau 1977; LMC: $0.07 \pm 0.01$, Brunet 1975). They are somewhat higher than, but still within the error bars of the values given by Koornneef (1984) and decidedly higher than the average values given by McNamara & Feltz (1980). The latter derived $E(B-V)$ from Galactic foreground stars which has the disadvantage that these are not numerous; in addition, they might not be distant enough to sample all Galactic foreground dust towards the Clouds. Indeed, use of stars inside the Magellanic Clouds (Isserstedt 1975) yields higher values of $E(B-V)$. There, all of the foreground is included, but the correction for contamination by Magellanic Cloud dust is somewhat uncertain. In addition, optical determinations of low extinction values strongly depend on accurate knowledge of intrinsic colours, which is particularly

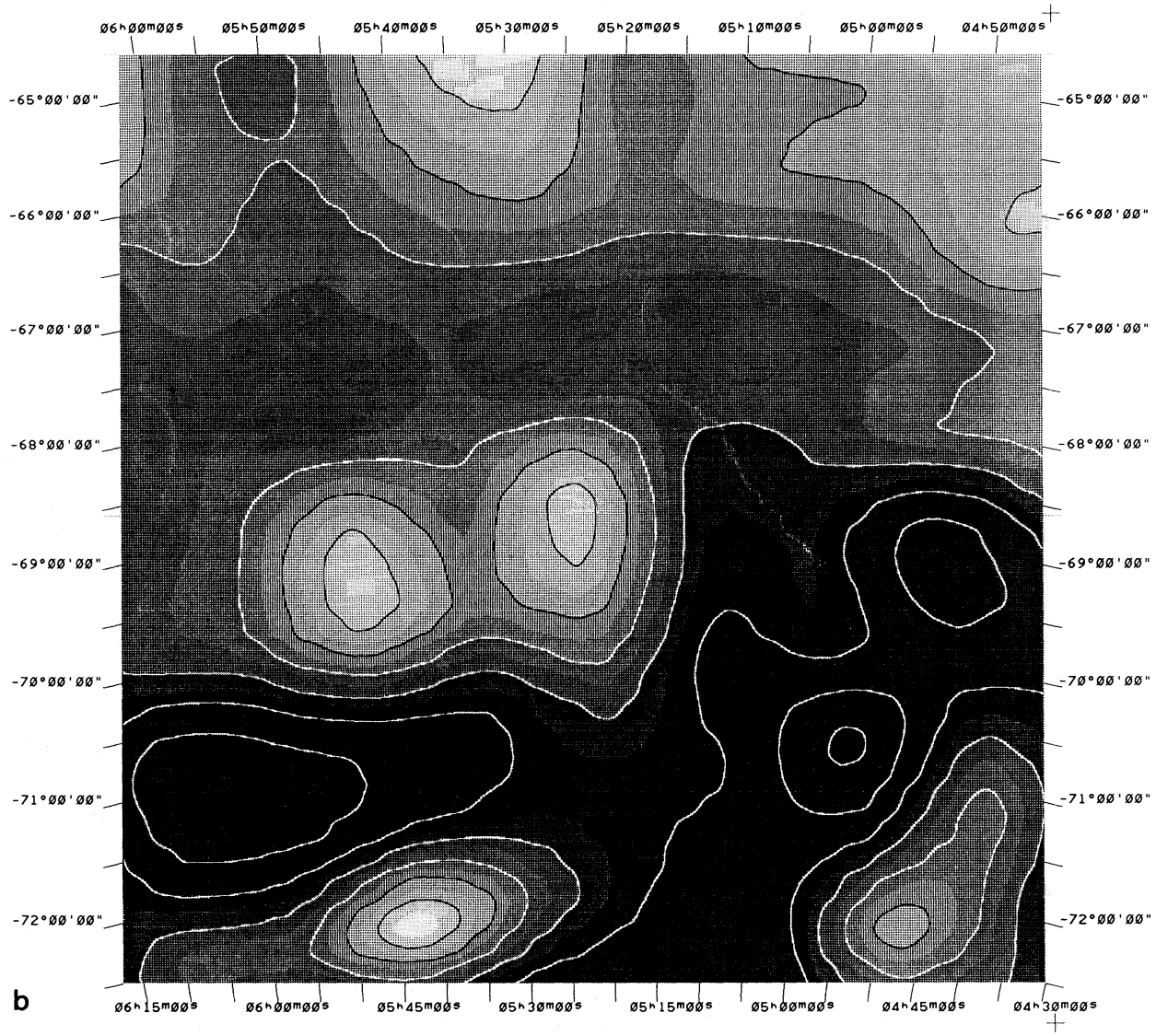


**Fig. 7b.** Map of Galactic foreground colour excess $E(B-V)$ towards the LMC. Contours range from 0.06 to 0.18 in steps of 0.02 mag. Grey scales are in steps of 0.01 mag

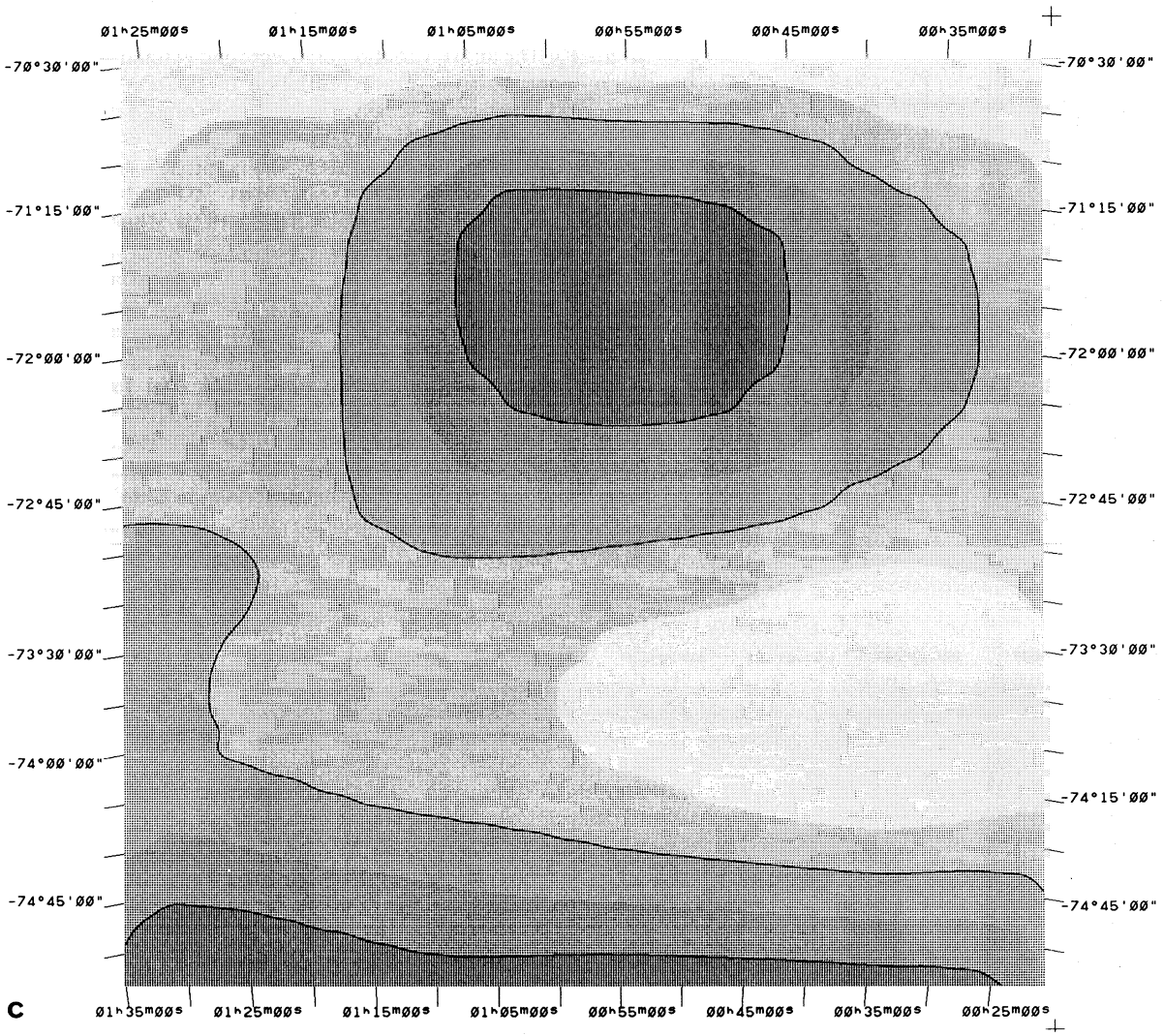


**Fig. 7c.** As in b, for the SMC. Contours are 0.08 and 0.10 mag; grey scales are in steps of 0.01 mag. The maximum at $\alpha = 00^h55^m$, $\delta = -72°0$ is due to noise blow-up

troublesome for Magellanic Cloud stars with metallicities lower than those of relatively well-studied Galactic stars.

The present method samples essentially all foreground material, without Magellanic contamination, but suffers from a coarse resolution. A limited check on our result is provided by the observations of 41 foreground stars in a roughly 3° field towards SN 1987A by Gochermann et al. (1989). They find foreground $E(B-V)$ values in the range 0.02 to 0.20 with a mean $E(B-V) = 0.08 \pm 0.01$. In addition, their Fig. 1 shows the highest reddening values to occur at locations where our Fig. 7 also indicates high mean reddening values. Thus, their results are in excellent agreement with ours, but they also imply considerable reddening structure on scales as small as 10 arcmin (i.e. 0.3 pc at a distance of 100 pc).

Significantly lower values of the mean foreground $E(B-V)$ are indeed unlikely, as can be seen as follows. If the lower values given by McNamara & Feltz (1980) were correct the H I foreground observations would imply ratios $N(\mathrm{H\,I})/E(B-V) =$ 16 $10^{21}$ and 23 $10^{21}$ H cm$^{-2}$ mag$^{-1}$ towards the LMC and SMC respectively, three to four times higher than the Solar Neighbourhood value given by Savage & Mathis (1979). Such values are comparable only to those of environments depleted in heavy elements, such as the dense Rho Oph cloud (7 $10^{21}$ H cm$^{-2}$ mag$^{-1}$; Savage & Mathis 1979), and the interstellar medium of the LMC itself (20 $10^{21}$ H cm$^{-2}$ mag$^{-1}$; Koornneef 1984).

## 5. Extinction inside the Magellanic Clouds

The extinction inside the LMC has been studied by Isserstedt (1975) and Isserstedt & Kohl (1984) on the basis of stellar photometry. Their database consists of LMC-stars of known colour, to which a constant foreground extinction correction of 0.07 mag is applied. We have shown that part of the LMC Bar and the Greater 30 Doradus region have relatively weak H I foregrounds, and are less obscured than outlying regions such as Shapley's Constellation III and the N 11 complex. The high values of $E(B-V) > 0.14$ mag found in 30 Doradus thus reflect mostly internal LMC extinction. In contrast, the LMC colour excess of stars at the periphery, and especially in the southern part of the LMC is overestimated by 0.03–0.07 mag. Here a large number of stars have published colour excesses $E(B-V) < 0.08$ mag (Isserstedt & Kohl 1984). Correction for the actual foreground decreases this to on average $E(B-V) < 0.04$ mag, but small-scale

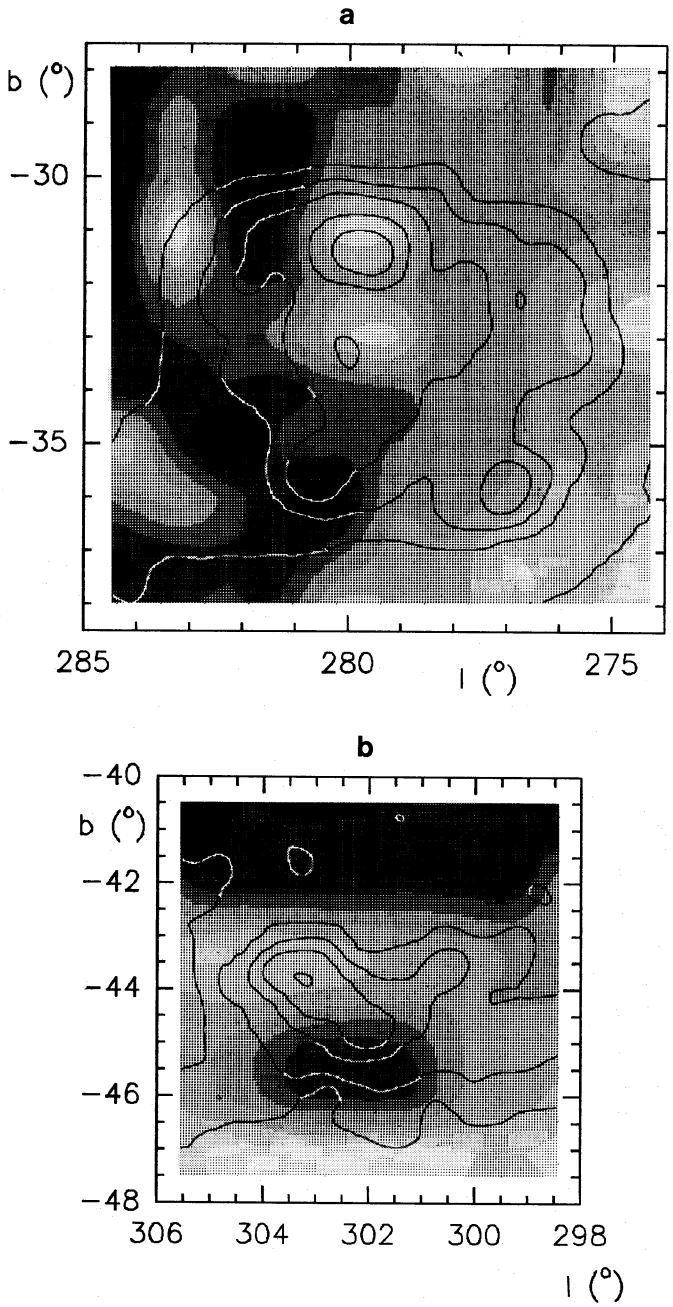


**Fig. 8.** **a** Contours of the 100 μm infrared emission of the LMC overlaid on halftone mag of the Galactic foreground $E(B-V)$ distribution. **b** As Fig. 7b, but for the SMC

variations will introduce considerable differences for *individual* stars (also noted by Isserstedt 1985). Because the smoothed foreground extinction is at least 0.05 mag, we do not expect more than a few stars in the LMC to have $E(B-V) < 0.04$ mag. Their apparent occurrence thus must be due to systematic errors such as those mentioned in the preceding section. Some indication for this is supplied by the presence of stars with $E(B-V) = -0.10$ in Isserstedt's (1985) diagram.

Fitzpatrick (1985, 1986) has presented a rather careful study of the spatial variation of the LMC interstellar extinction curve. He finds the "average" LMC extinction curve to be less extreme than that of the 30 Doradus region (which in turn resembles the extinction curve derived by Koornneef & Code 1981). The latter (often referred to as the "LMC extinction curve") has a considerable weaker 2200 Å feature and exhibits a steeper rise in the ultraviolet than the standard Galactic curve. By assuming the foreground contribution to the observed colour excess not to vary, Fitzpatrick concludes that his new LMC curve is a better average than the 30 Doradus curve, which then must resemble an abnormal part of the LMC. However, our finding that the foreground extinction varies systematically over the LMC forces a reconsideration of this conclusion (as Fitzpatrick 1985 himself acknowledged it would).

For his extinction determinations, Fitzpatrick (1985, 1986) used comparison stars located as much as 2° distant from the target stars, with clearly different foreground $E(B-V)$, thus introducing *systematic* errors up to twice the random photometric uncertainty of 0.02 mag. Because of the very low foreground extinction of 30 Doradus, and the higher than average extinction especially in the south, but also in the north, extinction curve differences between the 30 Doradus region and other parts of the LMC are artificially enhanced. We have determined actual (but low resolution) foreground extinctions of both the reddened and "unreddened" stars in Fitzpatrick's sample, and corrected his intrinsic LMC reddening values for the difference in foreground extinction between sample star and comparison star. The results are as follows: the non-Doradus stars in the 1985 sample have on average reddening values about 10% higher than listed, whereas the stars in the 1986 sample have on average reddening values about 10% lower. The average (non-Doradus) LMC extinction curve thus needs very little change. This is not true for the 30 Doradus sample in the 1985 study. Here, the comparison stars, located in the north of the LMC, suffer systematically $E(B-V) = 0.03$ mag more foreground extinction than the 30 Doradus stars themselves. This corresponds to a *systematic* underestimate of 30 Doradus $E(B-V)$ values of slightly more than 20%. When the 30 Doradus extinction curve is corrected for this amount, its deviation from the standard Galactic curve becomes less pronounced, and in fact it is very similar to Fitzpatrick's (1986) "average" LMC curve.

We note that the star Sk 52–71 is located in a region of rather high foreground reddening; its LMC-extinction appears to be about 0.05 mag less than found by Fitzpatrick (1985), making its extinction curve even more extreme. In interpreting this result one should, however, be cautious as the poor resolution of the foreground extinction map allows proper application only to large samples. Good statistics are essential as small-scale foreground structure complicates matters considerably (cf. Gochermann et al. 1989). We emphasize that stars located in the eastern Bar and in the Greater 30 Doradus region are in principle most suited to LMC extinction curve determinations as there the confusing influence of the Galactic foreground is, at least statistically, less than elsewhere.

The SMC extinction curve (Prevot et al. 1984) is more extreme. The 2200 Å feature is almost completely absent and the far-UV rise is very steep. However, Lequeux et al. (1984) have identified the SMC stars Sk 124, Sk 191 and especially Sk 143 as having extinction curves similar to the standard Galactic curve. Although our data provide no reason to expect a high Galactic foreground contribution to precisely these stars, the presence of significant (small scale) extinction variations in the LMC foreground suggests that similar variations may be present in the SMC foreground. Because of the lower *internal* extinction of the SMC, such foreground variations would have a commensurably more important effect on derived SMC extinction curves.

## 6. Conclusions

1. The diffuse infrared Galactic foreground of the Magellanic Clouds shows substantial structure. It has a fairly constant temperature $T_d = 21 \pm 2$ K. Between $b = -10°$ and $b = -35°$ $T_d$ decreases away from the Galactic plane.

2. At least for the LMC, the infrared foreground predicted from H I observations provides a better fit to the data than a flat foreground. At 60 μm the foreground contributes 10–20% to the emission of the Clouds over the same area; at 100 μm this is 30–40%. The foreground is more important for the SMC.

3. The infrared foreground is well-correlated with the neutral hydrogen column density $N$(H I), but the relation is non-linear. At 100 μm the dependence on $N$(H I) appears to be quadratic. The field-averaged ratio $I_{100\,\mu m}/N(\mathrm{H\,I})$ is $(0.6 \pm 0.2)\ 10^{-20}$ MJy sr$^{-1}$ cm$^2$.

4. Towards the LMC, foreground reddening shows structure down to the resolution limit (48 arcmin); structure on even smaller scales is evident from optical work. In front of the LMC, $E(B-V)$ ranges from 0.05 to 0.17 mag, and in front of the SMC from 0.06 to 0.08 mag. Foreground reddening towards 30 Doradus and the eastern LMC-Bar is lower than average.

5. With this result, we find little difference between the ultraviolet extinction curves of 30 Doradus and the rest of the LMC; the 30 Doradus extinction curve then deviates somewhat less from the Galactic extinction curve than previously thought.

## References


Albada van G.D., Baud B., de Pagter P.J., Pol W., Renes J.J., Wesselius P.R., 1985, ROG Internal Report
Azzopardi M., Vigneau J., 1977, A&A 56, 15
Bohlin R.C., Savage B.D., Drake J.F., 1978, ApJ 224, 132
Bloemen J.B.G.M., Deul E.R., Thaddeus P., 1990, A&A 233, 437
Boulanger F., Perault M., 1988, ApJ 330, 964
Brunet J.P., 1975, A&A 43, 345
Burton W.B., Deul E.R., 1987, in: The Galaxy, eds. G. Gilmore, R. Carswell, Reidel, Dordrecht, p. 141
Cleary M.N., Heiles C., Haslam C.G.T., 1979, A&AS 36, 95
Colomb F.R., Poppel W.G.L., Heiles C., 1980, A&AS 40, 47
Cox P., Krugel E., Mezger P.G., 1986, A&A 155, 380
Dame T.M., Thaddeus P., 1987, ApJ 297, 571
de Geus E., 1988, Ph.D. Thesis, University of Leiden
de Vaucouleurs G., 1955, AJ 60, 126
de Vries C.P., 1986, Ph.D. Thesis, University of Leiden
Deul E.R., 1988, Ph.D. Thesis, University of Leiden
Deul E.R., Burton W.B., 1990, A&A 230, 153
Deul E.R., Wolstencroft R.D., 1988, A&A 196, 277
Draine B.T., Lee H.M., 1984, ApJ 285, 89
Draine B.T., Anderson N., 1985, ApJ 292, 494
Fitzpatrick E.L., 1985, ApJ 299, 219
Fitzpatrick E.L., 1986, AJ 92, 1068
Gochermann J., Goudfrooy P., Schmidt-Kaler Th., 1989, A&A 213, 333
Heiles C., Cleary M.N., 1979, Aust. J. Phys. Suppl. 47
Hildebrand R.H., 1983, Q. J. R. Astron. Soc. 24, 267
IRAS: 1988, Catalogs and Atlases, Vol. 1, Explanatory Supplement, eds. C.A. Beichmann, G. Neugebauer, H.J., Habing, P.E. Clegg, T.J. Chester, NASA RP-1190
Israel F.P., Schwering P.B.W., 1986, in: Light on Dark Matter, ed. F.P. Israel, Reidel, Dordrecht, p. 383
Isserstedt J., 1975, A&A 41, 175
Isserstedt J., Kohl W., 1984, A&A 139, 115
Johnson P.G., Meaburn J., Osman A.M.I., 1982, MNRAS 198, 985
Koornneef J., 1984, in: Structure and Evolution of the Magellanic Clouds, IAU Symp. 108, eds. S. van den Bergh, K.S. de Boer, Reidel, Dordrecht, p. 333
Koornneef J., Code A.D., 1981, ApJ 247, 860
Lequeux J., Maurice E., Prevot L., Prevot-Burnichon M.-L., Rocca-Volmerange B., 1984, in: Structure and Evolution of the Magellanic Clouds, IAU Symp. 108, eds. S. van den Bergh, K.S. de Boer, Reidel, Dordrecht, p. 405
Lockman F.J., Jahoda K., McCammon D., 1986, ApJ 302, 432
May J., Murphy D.C., Thaddeus P., 1990, A&AS (submitted)
McGee R.X., Newton L.M., 1981, Proc. Astron. Soc. Aust. 4, 189
McGee R.X., Haynes R.F., Grognard R.J.-M. Malin D., 1986, Mon. Not. R. Astron. Soc. 221, 543
McNamara D.H., Feltz K.A., 1980, Publ. Astron. Soc. Pac. 92, 587
Osterbrock D.E., 1973, Astrophysics of Gaseous Nebulae, Freeman, San Francisco, p. 181
Prevot M.L., Lequeux J., Maurice E., Prevot L., Rocca-Volmerange B., 1984, A&A 132, 389
Puget J.L., Leger A., Boulanger F., 1985, A&A 142, L19
Rohlfs K., Kreitschmann J., Siegman B.C., Feitzinger J.V., 1984, A&A 137, 343
Savage B.D., Mathis J.S., 1979, ARA&A 17, 73
Schwering P.B.W., 1988, Ph.D. Thesis Leiden University (NL)
Strong A.W., Riley P.A., Osborne J.L., Murray J.D., 1980, MNRAS 201, 495
West R.M., Pedersen H., Madsen C., 1987, ESO Messenger no. 50, p. 24